Electric Power Systems Research 224 (2023) 109765

Contents lists available at ScienceDirect

Electric Power Systems Research

journal homepage: www.elsevier.com/locate/epsr

# Estimating distance to transient and restriking earth faults in high-impedance grounded, ring-operated distribution networks using current ratios ☆

Thomas Treider *, Hans Kristian Høidalen

*Department of Electric Energy, Norwegian University of Science and Technology, Trondheim, Norway*

ARTICLE INFO

*Keywords:*
Closed-ring networks
Earth faults
Fault location
Intermittent faults
Restriking faults

ABSTRACT

Earth faults occur frequently in distribution networks, and in resonant grounded networks they are challenging to locate precisely due to their naturally low fault current. Transient and restriking faults are more challenging still due to the short time available for the fault location logic, as well as the absence of steady-state conditions. This paper investigates the performance of three fault location methods utilizing the ratios of various current components in a network operated in a closed-ring configuration. A frequency dependent model of a distribution network is used to simulate transient and restriking faults, and both isolated grounding and resonance grounding are considered. The results show that fault location based on negative-sequence currents is able to locate transient faults, and its accuracy of a few hundred metres is comparable to what has been observed during permanent faults. A zero-sequence method is observed to be less accurate, particularly in resonant grounded networks. A transient method is also proposed, and while it is fast, it is ultimately limited by the presence of loads and branches in the network. It is concluded that the negative sequence method is best suited for transient and restriking faults.

## 1. Introduction

Earth faults are the most common fault type in distribution networks, and 50%–80% of faults in the Nordic countries are of this type [1]. Because the earth fault current is naturally low in small isolated networks, or made low in resonant grounded networks, earth faults have always represented a challenge for the protection and fault location systems in these networks. Due to the unique properties of isolated and resonant grounded networks, earth faults require an entirely different analysis than what can be applied in solid grounded networks. Protection principles such as distance protection and overcurrent protection are not suited due to the low fault current levels, and the fault location process is usually limited to the identification of the faulted feeder or section based on directional earth faults relays or fault passage indicators (FPIs). Furthermore, transient and restriking or intermittent faults represent one sub-category of earth faults which are notoriously challenging to locate. These faults are very common in distribution networks, particularly in resonant grounded cable networks [2], and they can often be the start of a more serious fault if not disconnected [3].

A variety of different approaches for detection and location of earth faults can be found in the scientific literature. Usually, the methods assume a radial networks and are often limited to locating the faulty feeder or section of the network. The use of the charge-voltage relationship of different feeders is proposed in [4,5], while estimation of the feeder capacitances is used to find the faulty feeder in [6,7]. Other directional transient principles exist which are supposed to be applicable in non-radial network as well, such as methods based on transient zero sequence energy [8,9]. In [10], a novel protection principle based on the charging transient is proposed specifically for meshed systems, where the angle between the zero sequence current and voltage is used as a directional element. By using a communication scheme and multiple relays the faulty line in a mesh can be determined, but the protection scheme requires relays on both ends of the line. The aforementioned methods are only able to determine the correct feeder or line, not the exact fault location. The authors of [11] present a comprehensive overview of the state-of-the-art for location of earth faults in distribution networks with isolated and compensated grounding schemes, demonstrating that accurate fault location in these networks is lacking. The available options are fewer still when considering transient and intermittent faults, in which case methods requiring steady-state conditions cannot be used. Refs. [12,13] are two examples of recently developed methods for detection and selective protection of intermittent faults in isolated and compensated

☆ The work was funded by the Norwegian Research Council project ProDig (295034/E20).

* Corresponding author.
*E-mail addresses:* thomas.treider@ntnu.no (T. Treider), hans.hoidalen@ntnu.no (H.K. Høidalen).

https://doi.org/10.1016/j.epsr.2023.109765
Received 4 April 2023; Received in revised form 27 July 2023; Accepted 9 August 2023
Available online 19 August 2023

**Nomenclature**

| | |
|---|---|
| $i_{a,A}(t)$ | Time domain current in phase $a$ on feeder A |
| $i_{a,B}(t)$ | Time domain current in phase $a$ on feeder B |
| $i_{a,sum}(t)$ | Sum of $i_{a,A}$ and $i_{a,B}$ |
| $I_{a,A}(f)$ | Frequency domain transform of $i_{a,A}$ |
| $I_{a,B}(f)$ | Frequency domain transform of $i_{a,B}$ |
| $I_{a,sum}(f)$ | Frequency domain transform of $i_{a,sum}$ |
| $f_{ch}$ | The frequency of the charging transient component |
| $\tilde{I}_{a,A}$ | $I_{a,A}$ evaluated at the charging transient frequency, i.e. $\tilde{I}_{a,A} = I_{a,A}(f_{ch})$ |
| $\tilde{I}_{a,A}$ | $I_{a,B}$ evaluated at the charging transient frequency, i.e. $\tilde{I}_{a,B} = I_{a,B}(f_{ch})$ |
| $\tilde{I}_{a,A}$ | $I_{a,sum}$ evaluated at the charging transient frequency, i.e. $\tilde{I}_{a,sum} = I_{a,sum}(f_{ch})$ |
| ASC | Arc suppression coil |
| DG | Distributed generation |
| FPI | Fault passage indicator |
| TW | Travelling wave |

networks, but accurate fault location capabilities are missing. Refs. [14–16] are examples of efforts into the development of a transient distance element which may be sufficiently fast for location of intermittent faults, but the presented results are sparse and their performance during intermittent faults is not demonstrated. Methods based on travelling waves (TW) are in theory very accurate and fast [17], but they are challenging to apply in distribution networks due to multiple reflection points, and research into this field is ongoing and not solved [11]. The authors of [11] highlight FPIs as a promising alternative for earth fault location and further develops this in [2], but the fault location accuracy is inherently limited by the spacing of the FPIs. While intermittent transient fault detection and selective protection is a standard feature in modern protective devices, accurate location of intermittent faults requires more research [11].

A closed-ring topology can be an alternative to the conventional radial topology commonly used in distribution networks [18]. Distribution networks are often built with the option of closed-ring operation to add flexibility during fault clearing events and network re-configurations. While a permanent transition to a closed-ring operation of the network will require an adjustment of the protection systems, it can be beneficial due to more balanced load and voltage profiles [19,20], it can save costs by reducing the need for grid expansion [20] and by reducing losses [21], and it has been shown to increase the network reliability [22]. A closed-ring operation of parts of the network can also be beneficial by facilitating new fault location solutions [18]. In [18], two fault location methods were proposed utilizing a novel current ratio principle which takes advantage of a closed-ring topology. These methods were based on the negative sequence currents and zero-sequence currents measured on the two ring-connected feeders, respectively, and their performance was evaluated for permanent earth faults. While the methods showed very good results in the case of permanent faults (faults located within a few hundred metres in most cases), their performance during transient and restriking faults has not been studied. In this paper, a more accurate frequency dependent line model is implemented so that this can be investigated. Furthermore, it is hypothesized that a specific earth fault transient can be used to implement the same basic fault location principle. Thus, a novel transient principle is proposed and investigated as well.

The rest of the paper is organized as follows. In Section 2 the two methods from [18] are summarized, the new transient version is derived, and their implementation is discussed in detail. Sections 3 and 4 presents the modelling and results from simulations using ATPDraw. The results are discussed and summarized in Section 5 before a conclusion is given in Section 6.

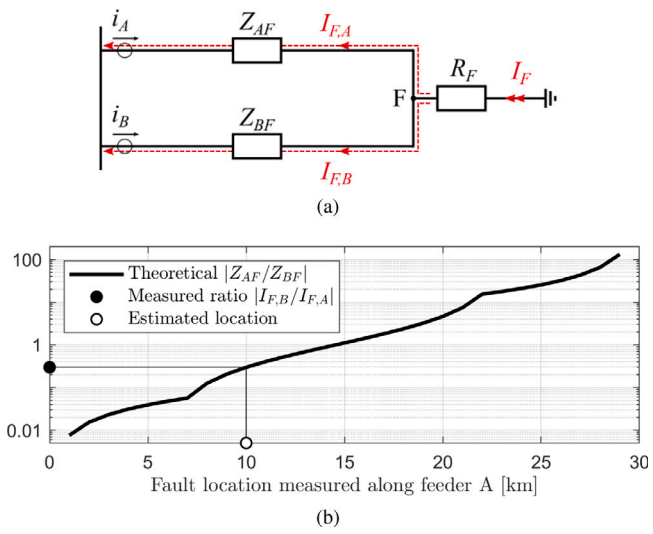


**Fig. 1.** (a) Division of the charging transient component in the faulty phase, and (b) converting an observed current ratio to a distance estimate on a 30 km long ring.

## 2. Fault location based on current ratios

In [18], two fault location methods based on current ratios were proposed, using either negative sequence or zero-sequence quantities. Generally, the current ratio principle can be explained by considering Fig. 1(a). The fault current $\vec{I}_F$ is divided in two components which are contained in the currents measured on the beginning of each of the two ring-connected feeders. By extracting these fault current components, their ratio can be used to estimate the ratio of the impedances between the fault and the measurements:

$$\frac{Z_{AF}}{Z_{BF}} = \frac{\vec{I}_{F,B}}{\vec{I}_{F,A}} \tag{1}$$

With knowledge of the impedance of the lines, the impedance ratio can be converted to a distance estimate. Fig. 1(b) illustrates this in the case of a ring with total length 30 km.

### 2.1. Using the negative sequence currents

The ratio of the negative sequence currents can be used to estimate the ratio of the negative sequence impedances, as shown in (2). The pre-fault values of the currents are removed by using the current increments $\Delta\vec{I}_{2,A}$ and $\Delta\vec{I}_{2,B}$, making the method robust against both large fault resistance and asymmetric loads in the network.

$$\frac{Z_{2,AF}}{Z_{2,BF}} = \frac{\Delta\vec{I}_{2,B}}{\Delta\vec{I}_{2,A}} \tag{2}$$

### 2.2. Using the zero-sequence currents

Using the same approach as for the negative sequence currents, the zero-sequence currents can be utilized as well. However, two modifications must be made. First, the zero-sequence impedance must be used instead of the negative sequence impedance. Secondly, the capacitive components in the zero-sequence currents are not canceled when using incremental values of the currents, and therefore they must be subtracted in some other way. It is shown in [18] that this can be

done using the neutral voltage $\vec{V}_n$, assuming that the total three-phase admittance of the two feeders and their branches $\bar{Y}$ is known. This gives the following equation for estimating the impedance ratio:

$$\frac{Z_{0,AF}}{Z_{0,BF}} = \frac{\Delta 3\vec{I}_{0,B} - \Delta\vec{V}_n m_B \bar{Y}}{\Delta 3\vec{I}_{0,A} - \Delta\vec{V}_n m_A \bar{Y}} \tag{3}$$

The factors $m_A$ and $m_B$ describe the division of the capacitive parts of the zero-sequence currents on the two feeders, and an analytical approach for their calculation is given in Appendix A.

### 2.3. Using the charging transient

The charging transient is a specific earth fault transient which is well known and described in the literature [14–16,23–26]. In a radial network, this transient flows from the fault in to the main transformer along the faulty phase. In a ring network, the same principle of current division will apply, meaning that this component can also be used to implement the current ratio principle.

Using the same approach as in [24], the charging transient behaviour in a ring-operated network can be derived. For simplicity, two unloaded feeders without any laterals connected to form a ring, as shown in Fig. 2(a), is assumed. The network is shown as ungrounded, but the same circuit is valid for a resonant grounded network as well when considering frequencies above the fundamental frequency [27]. It is further assumed that the charging current is divided along these two paths according to the principle of current division, and that the resistance in the circuit can be neglected so that $Z \approx \omega L$. The sum of currents in these two paths then meets a parallel connection of the inductances in the two paths, $L_{eq}$:

$$L_{eq} = \frac{L_{AF} L_{BF}}{L_{AF} + L_{BF}} \tag{4}$$

The network in Fig. 2(a) can be represented by the LC-circuit in Fig. 2(b). By using $L_{eq}$ to represent the ring, the charging frequency can be estimated by (5).

$$f_{ch} = \frac{1}{2\pi\sqrt{(1.5L_T + L_{eq})(2C_g + 2C_p)}} \tag{5}$$

Because the value of $L_{eq}$ varies with the fault location, so does $f_{ch}$. Eq. (5) shows that the minimum frequency occurs approximately on the middle of the ring, where $L_{eq}$ reaches its maximum value, while the maximum frequency occurs for faults at the main bus, for which $L_{eq} = 0$.

When a fault occurs somewhere on two ring-connected feeders, the division of the charging transient among feeders A and B depends on the ratio of the impedances faced in the two paths. Assume that the fault occurs in phase $k$. Let $\tilde{I}_{k,A}$ and $\tilde{I}_{k,B}$ be the charging transient components of the phase currents $i_{k,A}$ and $i_{k,B}$ measured on feeders A and B, respectively. $Z_{k,AF}$ and $Z_{k,BF}$ are the self-impedances of the faulty phase in the two paths, evaluated at the charging frequency $f_{ch}$. With these modifications, the current ratio in principle can be implemented as described by (6).

$$\frac{Z_{k,AF}}{Z_{k,BF}} = \frac{\tilde{I}_{k,B}}{\tilde{I}_{k,A}} \tag{6}$$

### 2.4. Implementation

The methods considered in this paper are only providing fault location, and it is assumed that an external fault detection stage has determined the time of the fault inception $t_0$, as well as the faulty phase.

The methods based on the negative and zero-sequence currents are described in [18], and their implementation is summarized by the flowchart in Fig. 3. The only setting to vary is the time $t_x$, measured from the time of fault inception, at which the fault location estimate for the two fundamental frequency methods should be extracted. This was not considered in detail in [18] because permanent faults allowed

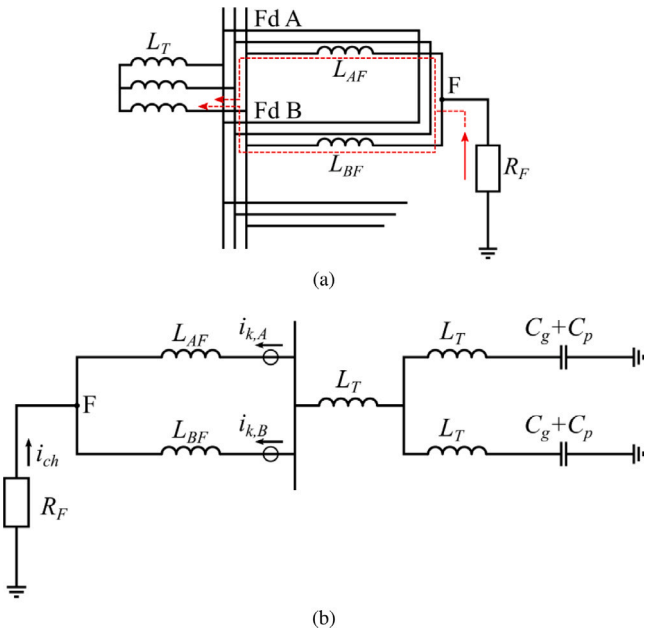


**Fig. 2.** Example of (a) two ring-connected feeders A, and B and (b) the equivalent LC-network for charging frequency estimation.

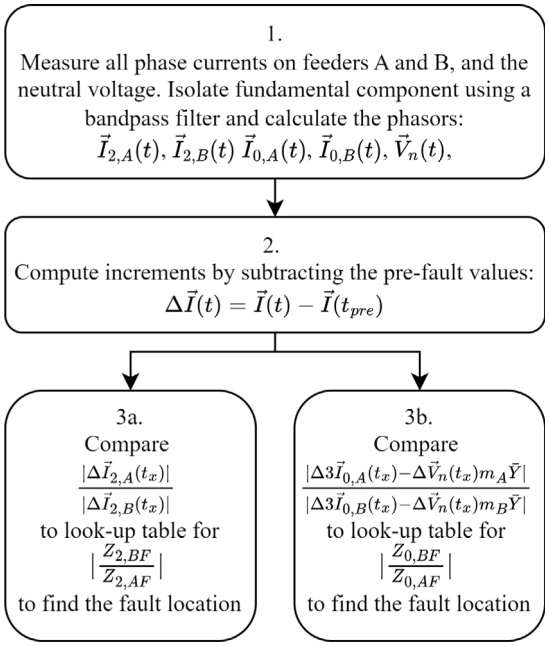


**Fig. 3.** Flowchart for the two methods in [18].

waiting for steady-state conditions. For transient faults however, the fault location estimate must be extracted in a few milliseconds after the fault. This parameter will be illustrated and discussed in more detail in Section 4.

The transient method requires more steps before a distance estimate is obtained. The entire process is summarized in Fig. 4, and the estimation of the charging transient frequency and the frequency dependent impedances is described in more detail in the following subsections.

#### 2.4.1. Estimating the charging transient frequency

Consider a fault occurring in phase $a$. In order to estimate the frequency of the charging transient, the sum $i_{a,sum} = i_{a,A} + i_{a,B}$ is used.

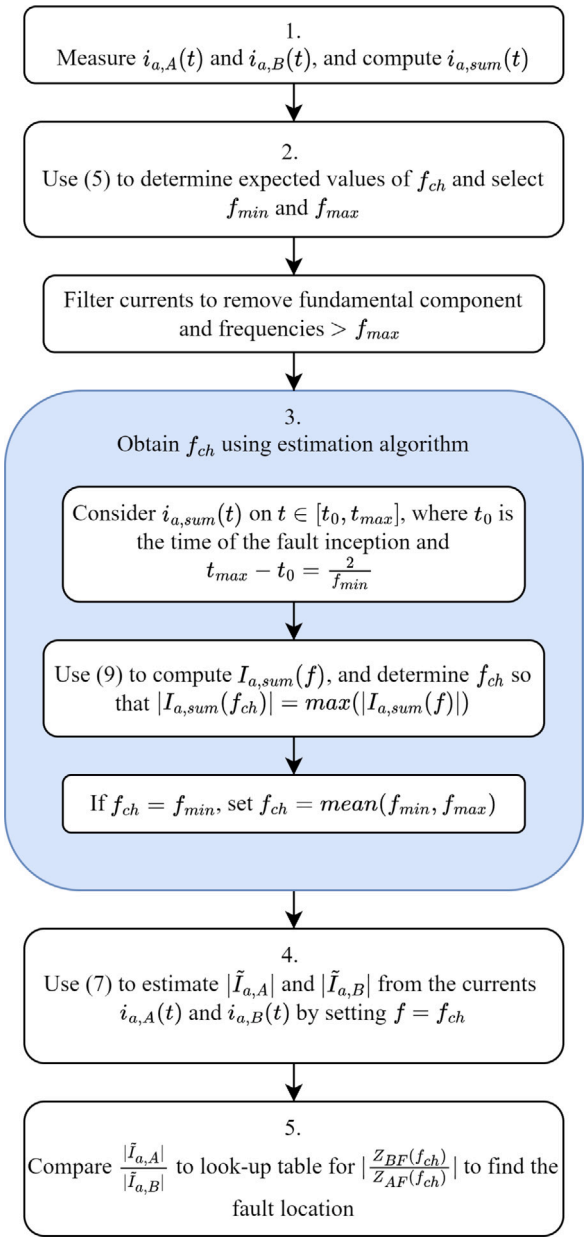


**Fig. 4.** Flowchart showing fault location in phase $a$ using the charging transient.

The sum of the currents is used to ensure that the charging transient component $\tilde{I}$ is present with a sufficient magnitude no matter where on the ring the fault is located, as either $\tilde{I}_{a,A}$ or $\tilde{I}_{a,B}$ will approach zero when the fault is located close to the main bus.

Before being transformed into the frequency domain, $i(t) = i_{sum,a}(t)$ is filtered to remove the fundamental frequency component as well as disturbing high frequency content. The time domain signal is transformed into the frequency domain using (7). Eq. (7) is applied on the frequency range $F = [f_{min}, f_{max}]$, which is selected by estimating the expected frequency range of the charging transient using (5) with the maximum and minimum values of $L_{eq}$.

$$I(f) = \sum_{t=t_0}^{t_{max}} i(t) \cdot e^{-j2\pi ft} \tag{7}$$

In (7), the current $i(t) = i_{sum,a}(t)$, $t \in [t_0, t_{max}]$. The frequency of the charging transient depends on the fault location and is not known in advance, and the length of the DFT-window, i.e. $T_{DFT} = t_{max} - t_0$, must therefore be long enough to accurately reproduce the lowest likely value of the charging transient frequency $f_{min}$. Therefore, the DFT-window is set to cover two periods of this frequency, i.e. $T_{DFT} = 2/f_{min}$. Fig. 5 illustrates the signal acquisition in the time domain.

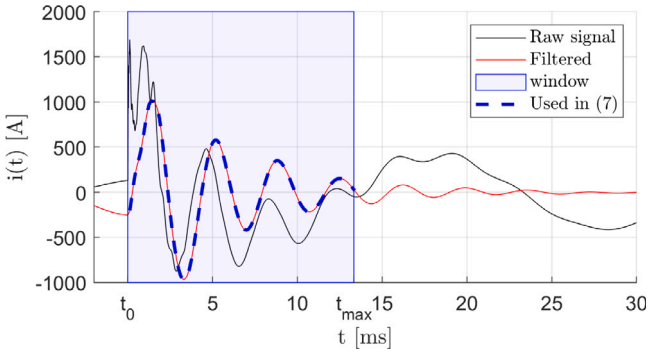


**Fig. 5.** Obtaining the current $i(t) = i_{sum,a}(t)$ used in (7) to estimate $f_{ch}$.

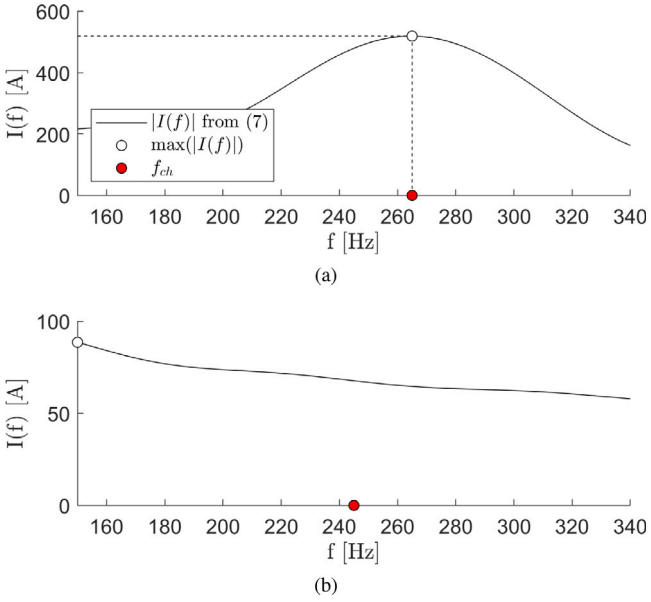


**Fig. 6.** Frequency spectrum and estimated charging frequency for (a) 1 Ω and (b) 15 Ω fault resistance.

The frequency corresponding to the maximum magnitude of $I(f)$ is chosen as an estimate of $f_{ch}$, as shown in Fig. 6(a). The fundamental frequency is not perfectly filtered out in practice, and when the fault impedance causes the charging transient magnitude to be reduced, the peak value of $|I(f)|$ will not correspond to the charging transient frequency. When this occurs, the maximum value of $|I(f)|$ will be found at $f_{min}$. To account for this, the above algorithm discards the estimate of $f_{ch}$ when it corresponds to $f_{min}$. Instead, the mean value of the frequency range considered is used to estimate $f_{ch}$. Fig. 6(b) illustrates how the transient becomes too small during a 15 Ω fault to be located with this approach. In this case, the mean frequency is used.

### 2.4.2. Estimating the frequency dependent impedance

In order to compare the measured ratio of the currents to the correct impedance ratio, the impedances at the correct frequency must be considered. Typically, it is the 50 Hz impedance $Z_{50\text{ Hz}}$ of the line which is known to the network operator. Estimating the frequency dependent impedance as $Z(\omega) \approx R_{50\text{ Hz}} + j\omega L_{50\text{ Hz}}$ is not accurate, and the frequency dependent values $R(\omega)$ and $L(\omega)$ should instead be estimated analytically. For overhead lines, (2.11), (2.12) and (2.27) or

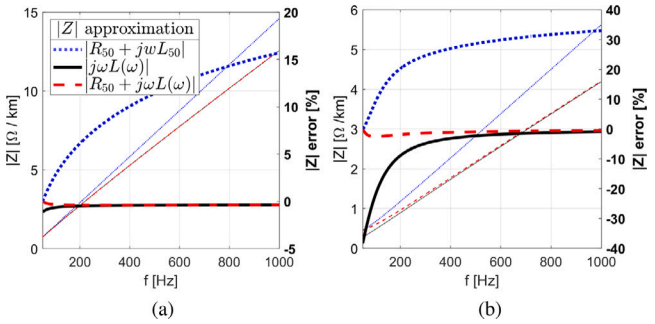


**Fig. 7.** Different approximations of the self impedance $|Z(\Omega)|$ for an (a) OH-line and (b) a cable, and their percentage errors (thick curves on right y-axis).

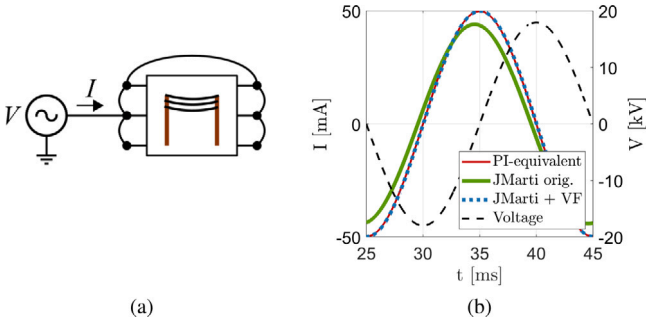


**Fig. 8.** (a) Simulation model for determining capacitive current to ground in a 1 km line segment, and (b) simulated currents with three different line models.

(3.23d) in [28] can be used to estimate the self impedance. For cables, Ref. [29] gives a detailed description of how to estimate the impedance. Fig. 7 shows that estimating $|Z(\omega)|$ using frequency independent parameters gives significant errors. In the case of the OH-line in Fig. 7(a), reasonable accuracy can be obtained using only the line inductance, whereas the cable in Fig. 7(b) with its higher R/X-ratio requires the inclusion of the resistance to avoid large errors at low frequencies. Fig. 7 also confirms that there is very little to gain from accounting for the frequency dependency of $R$ given that $\omega L(\omega)$ dominates at higher frequencies.

## 3. Modelling

### 3.1. Line model for studying earth fault transients

To study both the fundamental frequency component as well as the charging transient, it is of interest to use a line model which accurately represents the line from 50 Hz and up to the charging transient frequency (approximately 300 Hz in the test network in this paper). Conventional travelling wave models work poorly at low frequencies, particularly when it comes to representing the capacitance of the lines. PI-equivalents can be accurate at 50 Hz, but they are in turn inaccurate at higher frequencies. However, some models can provide frequency dependent line parameters and at the same time represent the capacitance with sufficient accuracy in the frequency range of interest [30–32]. The model in [30] combines JMarti and vector fitting (VF) and is implemented in ATPDraw version 7.4. Compared to the regular JMarti model, it has the benefit of being accurate in lower frequency ranges. Fig. 8 shows how the regular JMarti model in ATPDraw fails to reproduce the correct capacitance at 50 Hz, whereas the model in [30] closely matches the PI-equivalent. Fig. 9 shows that the line model also impacts the earth fault transients of interest. A network with 5 × 20 km OH-lines was modelled using the three different line models discussed previously. It can be seen that the PI-equivalent has too little damping, and the constant parameters result in the charging frequency being too low (here ≈ 650 Hz). The two JMarti models have similar responses, but over a few periods it is apparent that both their magnitudes and frequencies are different. Based on Figs. 8 and 9, the JMarti model in [30] is preferred.

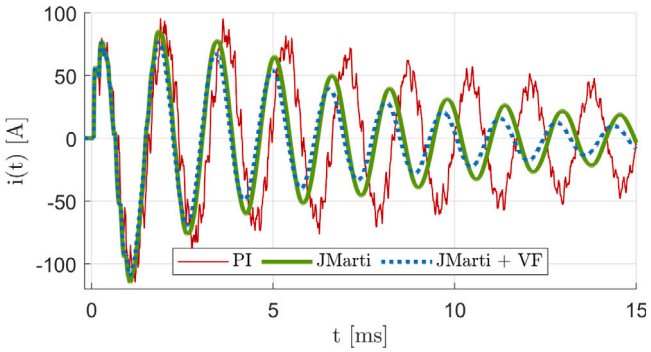


**Fig. 9.** Earth fault transient with different line models.

### 3.2. Test network

The test network used to verify the proposed fault location method is the network shown in Fig. 10, which is based on data from a Norwegian network operator, and the topology corresponds to the test network used in [18]. The network can be operated either with a resonant grounded or isolated grounding scheme, and the DG-units are disconnected unless otherwise stated. According to (5), the charging transient frequency is expected to vary between 187 Hz and 284 Hz for different fault locations on the ring. Adding a 20% security margin, the frequency range $F = [150\ \text{Hz}, 340\ \text{Hz}]$ is considered when applying (7). Note that the source impedance of the supplying network, transformed to the 22 kV-side of the transformer, has been included in $L_T$ when applying (5).

The model in [30] is used to represent the OH-lines and cables in the network. The positive and zero-sequence line parameters at 50 Hz are found through measurements (i.e., using ATPDraw's Line Check feature [33]), and the self impedance $Z_{50\ \text{Hz}}$ is derived from these values. With Line Check available, it could be used to estimate $L(\omega)$ directly, but in this case $L(\omega)$ is estimated from $L_{50\ \text{Hz}}$ using the analytical formulae referenced in 2.4.2. The frequency dependent impedance is then approximated as $Z(\omega) = R_{50\ \text{Hz}} + j\omega L(\omega)$.

### 3.3. Modelling faults

The permanent faults are modelled by connecting a resistance between the faulty phase and ground using a time-controlled switch, while the transient and-striking faults are modelled using a voltage dependent switch. This switch connects the faulty phase to ground via the fault resistance when the voltage over the switch exceeds the flashover voltage $V_{flash}$ of the switch, and it opens when the fault current drops below a set threshold $I_{mar}$. This results in the duration of each fault and the time between restrikes varying depending on the flashover voltage, the fault resistance and the grounding scheme.

## 4. Results

A variety of fault scenarios are used to test the three methods. The validity of the new transient method is first investigated separately using permanent faults, after which all three methods are tested for transient and restriking faults. See Appendix B for complete data and settings.

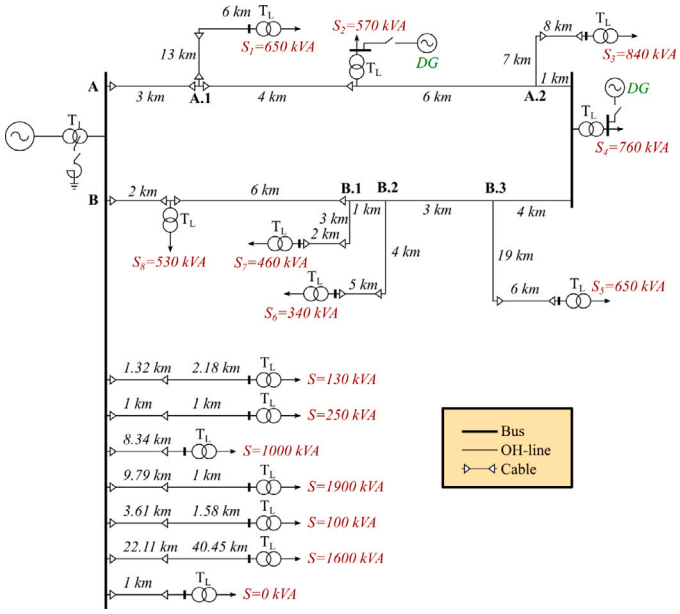


**Fig. 10.** Single line diagram of simulated network.

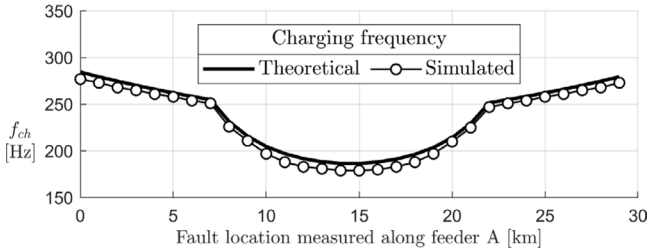


**Fig. 11.** Theoretical frequency predicted by (5), and observed frequency in the base case network.

### 4.1. Accuracy of the charging transient ratio

First, the novel transient method is investigated with a set of permanent 1Ω faults applied in phase $a$ in sequence at various fault locations around the ring. Fig. 11 shows the observed charging transient frequency for different fault locations on the ring. The figure also shows the theoretical values predicted by (5), illustrating that the LC-circuit in Fig. 2(b) is a reasonable approximation for the purpose of estimating the frequency. Note that the frequency dependency of the line inductance was accounted for when computing the theoretical frequency in Fig. 11, but very little change (< 2.7%) was observed when using its 50 Hz-value.

Fig. 12(a) shows that the transient method successfully estimates the impedance ratio, but the presence of loads and lateral branches on the ring reduces the accuracy. It can be seen that connecting the loads directly on the ring by removing lateral in between (labelled "Loads, no laterals" in Fig. 12) improves the accuracy, showing that it is the laterals themselves as well as the load which disturb the results. The exact mechanism involved has not been investigated in detail, but simulations have shown that each lateral contributes with an induced transient current at the charging frequency proportional to the amount of capacitance on that particular lateral. The loads themselves have the biggest impact on the results, however, and the effect of loads is to provide the transient with another path then the one assumed in Fig. 2(a). This creates significant errors close to the edges of the ring due to the fact that either $\tilde{I}_{a,A}$ or $\tilde{I}_{a,B}$ should approach zero as the fault moves towards the main bus, making the ratio between them susceptible to even small errors in the estimation of the magnitudes.

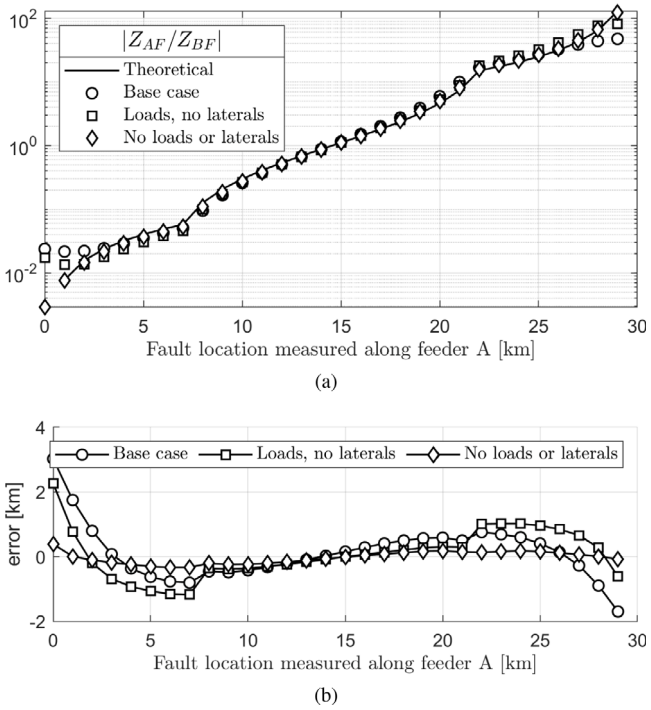


**Fig. 12.** (a) Estimated $|Z_{AF}/Z_{BF}|$-ratio and (b) corresponding distance estimate errors for the transient method.

### 4.2. Speed of the fundamental frequency methods

Fig. 13 shows how the impedance ratio estimates vary with time during a permanent fault. The negative sequence method reaches its final value much faster than the zero-sequence methods does, allowing a lower value of $t_x$. The zero-sequence estimate is very sensitive to even small differences in the current and voltage transients, resulting in very large variations in the estimate before steady state is reached. The negative sequence current has an equally long transient period, but because both $\Delta\vec{I}_{2,A}$ and $\Delta\vec{I}_{2,B}$ display a similar transient dynamic, the ratio between them stabilizes much earlier than the zero-sequence method does.

Fig. 14 illustrates how different settings of $t_x$ impacts the accuracy of the negative sequence method during transient faults, and similar results apply for the zero-sequence method as well. The highest value of $t_x$ gives good accuracy in Fig. 14(a), where the restrikes are regular and frequent. In Fig. 14(b), the situation is reversed. There, the network is resonant grounded, leading to longer intervals between restrikes. This occurs due to the much slower build-up of the phase voltage between strikes in the resonant grounded network [34], which is illustrated clearly in the example in Fig. 15. For the remainder of the paper, $t_x$ = 5 ms is used.

### 4.3. Restriking faults distance estimates

Figs. 16–19 show how the fault resistance impacts the three methods during transient faults in both an isolated and a resonant grounded network. The negative sequence method works best and is not significantly affected by the fault resistance, grounding scheme or flashover voltage. The transient method works best for low-ohmic faults and low flashover voltages, but it is still the less accurate then the negative sequence method. The zero-sequence method varies greatly, where the main issue is seen to be the grounding scheme. It works reasonably well in the isolated network (although less accurate than the negative

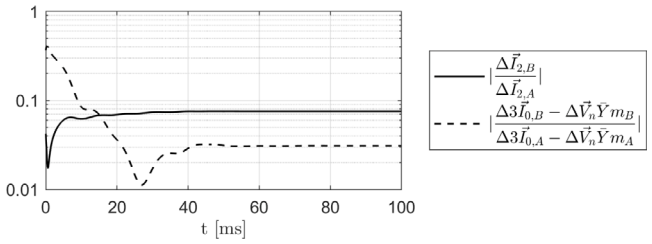


**Fig. 13.** The two ratios during a permanent 1 Ω fault occurring at $t = 0$ at point A.1 in Fig. 10 with the network operating with an isolated neutral point.

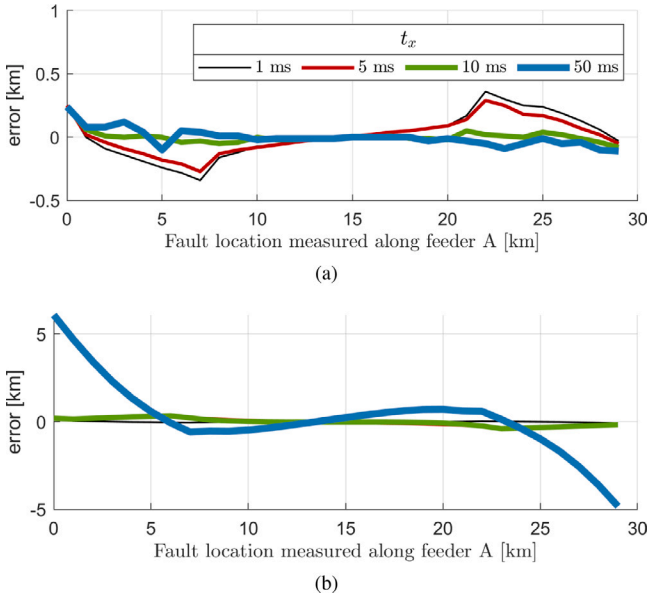


**Fig. 14.** The impact of $t_x$ on the negative sequence method's fault distance estimate for restriking faults in (a) an isolated network and (b) a resonant grounded network. $V_{flash}$ = 16 kV.

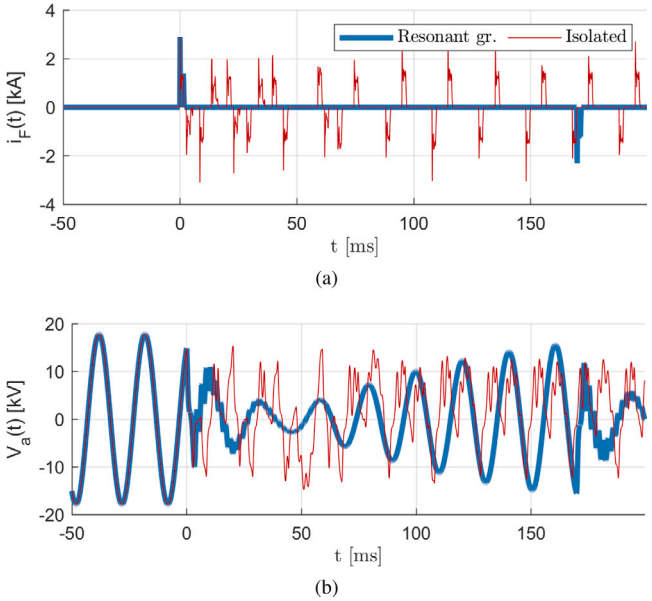


**Fig. 15.** Comparison of (a) fault current and (b) main bus faulty phase voltage during restriking fault at location A.1 in Fig. 10. $V_{flash}$ = 16 kV.

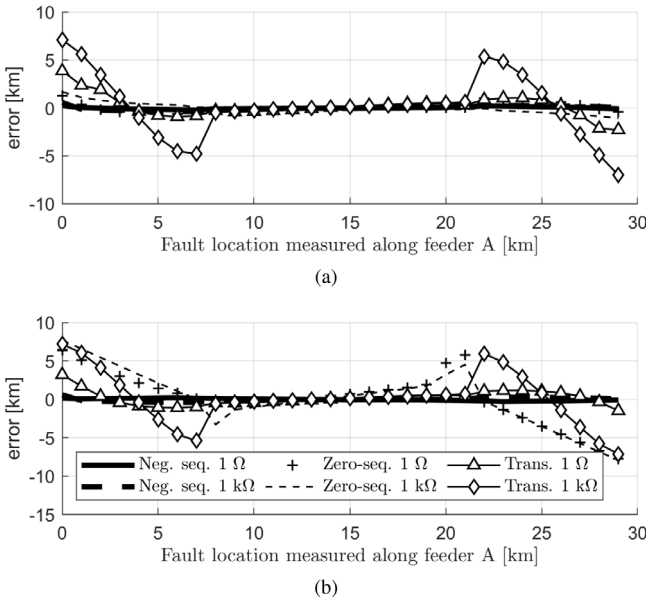


**Fig. 16.** Faults with flashover voltage 1.8 kV and 1 Ω or 1 kΩ in (a) isolated network and (b) resonant grounded network.

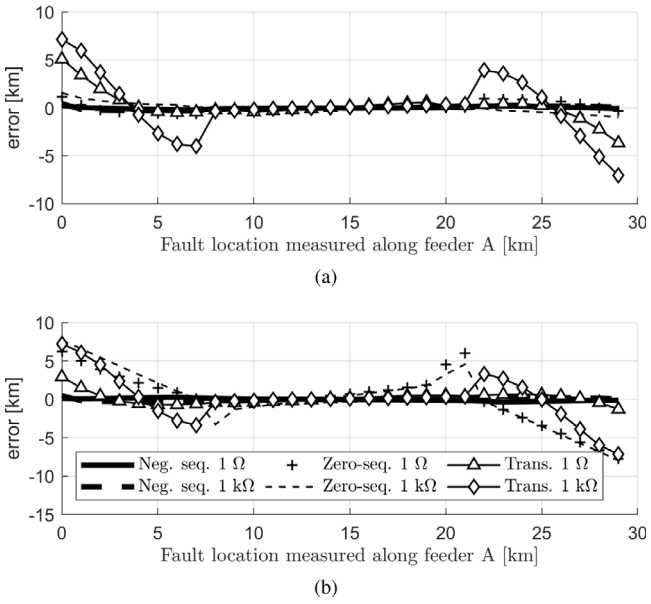


**Fig. 17.** Faults with flashover voltage 4.5 kV and 1 Ω or 1 kΩ in (a) isolated network and (b) resonant grounded network.

sequence method), but it is severely reduced in the resonant grounded network. For the cases in Figs. 16–19, the mean and maximum absolute errors were {0.13 km; 0.64 km} for the negative sequence method, {1.52 km; 10.35 km} for the zero-sequence method, and {1.38 km; 7.26 km} for the transient method.

### 4.4. Impact of harmonics and measurement noise

Next, permanent faults in the isolated network is considered, with $t_x$ = 5 ms. Fig. 20 shows the results of 500 randomly selected combinations of DC-components, fifth and seventh harmonics added to the two current measurements, and noise added to the neutral voltage. The DC-component has a value between ±5% of the pre-fault load current, whereas the two harmonics have magnitudes between 0%–5% and phase angles between 0°–360°. In addition, random noise have

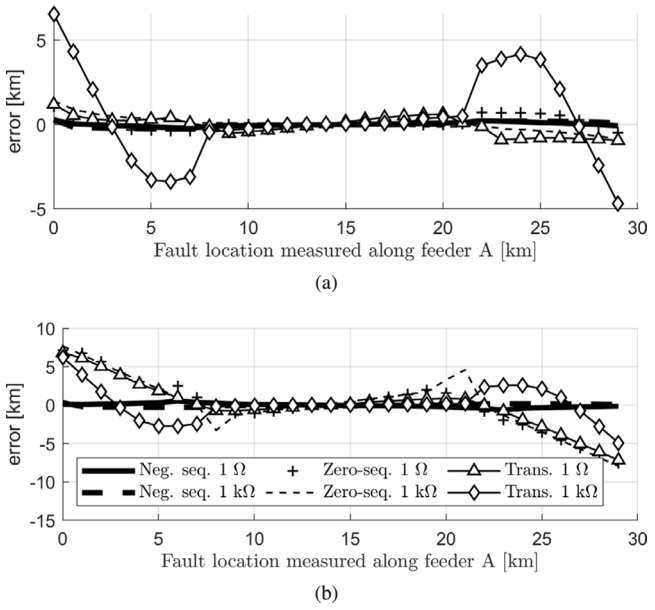


**Fig. 18.** Faults with flashover voltage 9 kV and 1 Ω or 1 kΩ in (a) isolated network and (b) resonant grounded network.

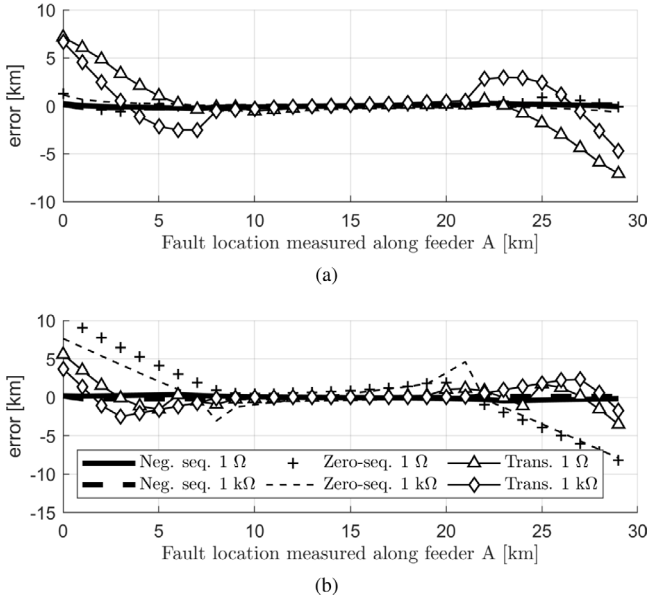


**Fig. 19.** Faults with flashover voltage 16 kV and 1 Ω or 1 kΩ in (a) isolated network and (b) resonant grounded network.

been added to each sample, with a magnitude between 0 and 5% of the actual magnitude at that sample. The blue areas in Fig. 20 show the envelope of all the resulting estimate errors for the three methods, along with the errors without harmonics or noise added (labelled "Base case"). It can be seen that the impact of noise and harmonics is negligible on the fundamental frequency methods, while the distance estimate changes by up to a few hundred metres in the case of the transient method.

## 5. Discussion

The results have shown that despite being based on fundamental frequency components and derived from a steady-state analysis, the

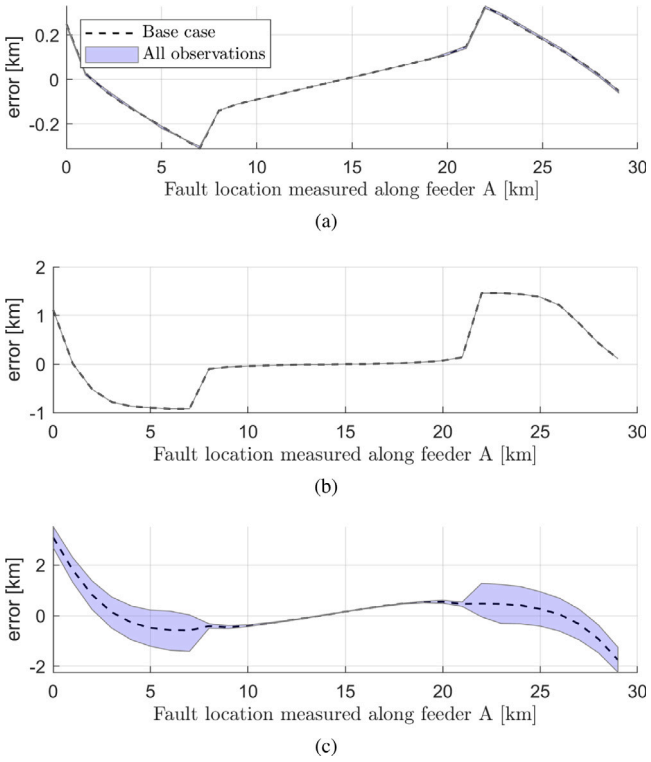


**Fig. 20.** Impact of harmonics and noise on (a) the negative sequence method, (b) the zero-sequence method and (c) the transient method.

methods based on the negative and zero-sequence currents can be applied to transient and restriking faults as well.

While the negative sequence method performs very well in both grounding schemes, the zero-sequence method is less accurate in the resonant grounded network. Though not included in the paper, similar results was observed for permanent faults. A possible explanation for this is that the fault current is much lower in the resonant grounded network compared to an isolated network of the same size. The capacitive parts of $\Delta 3\vec{I}_0$, i.e. $\Delta\vec{V}_n\bar{Y}$, is increased relative to the fault current, making the method more susceptible to small errors in the estimation and removal of this component. $\Delta\vec{I}_2$, however, consists mainly of the fault current, and faults in the resonant grounded network therefore resemble high impedance faults in the isolated network, for which this method is known to be robust [18].

It was also hypothesized at the beginning of this paper that the charging transient could be used to implement a similar current ratio principle. While the results demonstrate that this is correct, this transient method is not feasible in practice. To give sufficient accuracy comparable to that of the two fundamental frequency methods, the ring must be without loads and branches. Furthermore, as it is based on the measurement of transients, it is limited to low-ohmic faults.

From [18] it is known that the negative sequence method is affected by DG units in the network as well, where the accuracy was observed to be reduced by 700 metres at most, while the zero-sequence method is not impacted by DG-units. It was also observed in the simulations performed in this paper that the presence of DG units in the network reduced the accuracy of the transient method by a few hundred metres for faults in the middle of the ring and up to 2 km for faults close to the main bus. The effect of DGs on the transient method is comparable to that of loads and branches as the DG units provide the transient with an alternative path, and more DG units therefore further increase this effect.

### 5.1. Alternative methods for fault location

As determined by the authors of [11], few methods for accurate location of transient and restriking faults exists. TW-based methods appear be both difficult and costly to apply in distribution networks, and conventional earth fault relays cannot determine the exact fault location. For impedance-based methods, the method in [14,16] seems to be a likely alternative to the methods presented in this paper. However, results from transient faults are lacking, and it is likely to face many of the same challenges as the transient method proposed in this paper as they both utilize the same transient component. Without a more detailed description of its correct implementation available, a quantitative comparison cannot be made in this paper. Ref. [2] also proposes FPIs. The benefit is that faults can be located on the lateral branches as well, a property which the current ratio method lacks, but the drawback is the high number of FPIs needed to obtain an accurate fault location. Using the current ratio methods in conjunction with FPIs on the lateral branches can therefore be a good solution.

## 6. Conclusion

This paper has investigated the performance of three different methods for location of transient and restriking earth faults based on current ratios in closed-ring distribution networks. Two of the methods are based on fundamental frequency negative sequence currents and zero-sequence currents, while a novel transient principle has been proposed.

Using a frequency dependent line model in ATPDraw, the analysis has shown that:

- The negative sequence method works best in all the cases considered, with a mean distance estimate error of 0.13 km during transient and restriking faults.
- The zero-sequence method can be an option in an isolated network, but not in a compensated network.
- The transient principle proposed can only compete with the negative sequence method when the ring-connected feeders have no loads or laterals connected to them, making it less suited for a distribution network.
- The transient method is affected by harmonics close to the charging transient frequency as these harmonics cannot be filtered out, although the reduction in accuracy was observed to be a few hundred metres at most. The other two methods are not impacted by harmonics in the currents as these can be filtered out without affecting the fundamental component.

The main advantage of the current ratio methods compared to other solutions is that only readily available measurements in a single substation are required, making them easy and cost-efficient to implement in existing networks without the need for communication networks. The main drawback with these methods is that faults on lateral branches connected to the ring appear at the connection points, requiring other solutions for precise fault location on the branch itself.

## CRediT authorship contribution statement

**Thomas Treider:** Conceptualization, Methodology, Software, Formal analysis, Investigation, Writing – original draft, Writing – review & editing, Visualization, Project administration. **Hans Kristian Høidalen:** Software, Writing – original draft, Writing – review & editing, Supervision, Funding acquisition.

## Declaration of competing interest

The authors declare that they have no known competing financial interests or personal relationships that could have appeared to influence the work reported in this paper.

## Data availability

No data was used for the research described in the article.

## Acknowledgement

The authors appreciate discussions with and advice from B. Gustavsen at SINTEF Energy Research.

## Appendix A. Estimating the parameters $m_A$ and $m_B$

**Table B.1**
Test network and model parameters.

| Network data | |
|---|---|
| *OH-lines* | Conductor geometry: radius 11.87 mm, DC resistance 0.1115 Ω/km, height tower/mid 7 m/6 m. Plane geometry, 2 m between conductors. Ground wire geometry: radius 3.84 mm, DC resistance 0.8 Ω/km, height tower/mid 5 m/4 m, vertical position 1 m. Ground resistivity 100 Ωm. Lines are transposed and skin effect is included. |
| *Cable* | Core radii 0 mm (inner) and 9.1 mm (outer), sheath radii 14.75 mm (inner) and 17.25 mm (outer), cable radius 18.95 mm. Conductor resistivity 2.65E−8 Ωm, Relative permittivity of insulation 2.3. Triangular configuration with snaking at 1 m depth. Ground resistivity 100 Ωm. |
| *Main transformer* | 100 MVA 132/22 kV Dy1 transformer. X = 6%, R = 0.25%. Modelled using the Hybrid transformer model in ATPDraw with typical values for inductance and resistance, no capacitance or core effects included. |
| *Load transformers* | 2 MVA 22/0.4 kV Dy1 transformer grounded on the LV-side. X = 5%, R = 0.78%. Modelled using the Hybrid transformer model in ATPDraw with typical values for inductance and resistance, no capacitance or core effects included. |
| *Loads* | Grounded Y-connected constant impedance loads with power factor 0.9. |
| *Source* | Line voltage 132 kV, source impedance $3.47 + j34.67\Omega$ corresponding to 500 MVA according to [35]. |
| *DG units* | $S = 0.85$ MVA, $V_{line} = 400$ V, $X = 0.15$ p.u. [36]. |
| *Arc suppression coil* | 5 A over-compensated. Resistor $R_p = 20 \cdot X_n$ added in parallel to emulate losses. |
| *Faults* | Permanent faults in phase $a$ with inception angle approximately 60°. Restriking faults are modelled using a voltage dependent switch in ATPDraw with $T - de = 1$ ms (minimum time the switch remains closed) and $I_{mar} = 1$ A (switch opens when $I_f < I_{mar}$). |
| Simulation, signal processing and filters | |
| Software: ATPDraw version 7.4. Filters: 3rd order Butterworth low-pass filter with 500 Hz cut-off frequency before sampling in ATPDraw. Sample rate: 8 kHz. High-pass filter for transient method: 5th order Butterworth with 100 Hz cut-off frequency. Band-pass filter for 50-Hz methods: Matlab-designed equiripple with Fstop1 = 0 Hz, Fpass1 = 40 Hz, Fpass2 = 100 Hz, Fstop2 = 150 Hz, Astop1 = Astop2 = 60 dB, Apass = 0.1 dB. | |

**Table B.2**
Positive and zero sequence line parameters obtained using ATPDraw's line check feature.

| | OH-line | Cable |
|---|---|---|
| $Z^+$ | 0.1077+j0.356 Ω/km | 0.152+j0.0997 Ω/km |
| $Z_0$ | 0.4587+j1.1604 Ω/km | 0.2072+j0.0535 Ω/km |
| $C^+$ | 10.492 nF/km | 263.98 nF/km |
| $C_0$ | 5.8376 nF/km | 261.5 nF/km |

This theory is from [18]: The ring is divided into $n$ zero-sequence PI-equivalents, chosen so that the magnitude of the zero-sequence series impedance for each PI-section is the same, i.e. $|z_1| = |z_2| = |z_3| = \cdots = |z_n|$. The total capacitance of PI-section $k$ is labelled $C_k$. Next, the parallel capacitances of adjacent PI-equivalents are summed, and $n+1$ capacitances $\tilde{C}_0 - \tilde{C}_n$ are defined in (A.1).

$$\tilde{C}_i = \frac{1}{2}\begin{cases} C_{i+1} & i = 0 \\ C_i & i = n \\ C_i + C_{i+1} & i = 1, 2, \ldots, n-1 \end{cases} \tag{A.1}$$

By assuming that all these capacitances experience the same voltage, $V_0$, and by applying the principle of current division, the expressions below for $m_A$ and $m_B$ can be derived:

$$m_A = \frac{\sum_{i=0}^{n} \tilde{C}_i \frac{n-i}{n}}{\sum_{i=0}^{n} \tilde{C}_i} \tag{A.2}$$

$$m_B = \frac{\sum_{i=0}^{n} \tilde{C}_i \frac{i}{n}}{\sum_{i=0}^{n} \tilde{C}_i} \tag{A.3}$$

The accuracy of $m_A$ and $m_B$ increases as $n \to \infty$. Laterals on the feeders are accounted for by summing their entire zero-sequence capacitance to the corresponding $\tilde{C}_i$.

## Appendix B. Network data

The network in Fig. 10 is implemented in ATPDraw with the data given in the figure and in Table B.1. The lines and cables are modelled using the version of JMarti given in [30], where the model is fitted from 1–$10^7$ Hz. The positive and zero sequence line parameters obtained using Line Check is given Table B.2, and they are used to compute the self impedance.

## References


[1] S. Hänninen, M. Lehtonen, Characteristics of earth faults in electrical distribution networks with high impedance earthing, Electr. Power Syst. Res. 44 (3) (1998) 155–161.

[2] A. Farughian, L. Kumpulainen, K. Kauhaniemi, P. Hovila, Intermittent earth fault passage indication in compensated distribution networks, IEEE Access 9 (2021) 45356–45366.

[3] A. Wahlroos, J. Altonen, J. Xavier, Can compensated networks be an alternate solution to reduce the risk of ground faults causing forest fires? in: 2021 74th Conference for Protective Relay Engineers, CPRE, College Station, TX, USA, 2021, pp. 1–34.

[4] G. Druml, R. Klein, O. Seifert, New adaptive algorithm for detecting low- and high ohmic faults in meshed network, in: 20th International Conference on Electricity Distribution, Prague, 2009, pp. 1–6.

[5] T. Henriksen, Faulty feeder identification in high impedance grounded network using charge-voltage relationship, Electr. Power Syst. Res. 81 (9) (2011) 1832–1839.

[6] M. Loos, S. Werben, M. Kereit, J.-C. Maun, Detection of single phase earth fault in compensated network with C0 estimation, in: 22nd International Conference and Exhibition on Electricity Distribution, CIRED 2013, 2013, pp. 1–4.

[7] M.F. Abdel-Fattah, M. Lehtonen, Transient algorithm based on earth capacitance estimation for earth-fault detection in medium-voltage networks, IET Gener. Transm. Distrib. 6 (2) (2012) 161–166.

[8] M. Loos, S. Werben, M. Kereit, J.-C. Maun, Fault direction method in compensated network using the zero sequence active energy signal, in: Eurocon 2013, 2013, pp. 717–723.

[9] Z. Gajić, S. Aganović, R. Pajunen, S. Zubić, Universal earth-fault protection method for high impedance grounded power system, in: 15th Int. Conf. Developments in Power System Protection, DPSP 2020, 2020, pp. 1–6.

[10] J.D.R. Penaloza, A. Borghetti, F. Napolitano, F. Tossani, C.A. Nucci, A new transient-based earth fault protection system for unearthed meshed distribution networks, IEEE Trans. Power Deliv. 36 (5) (2021) 2585–2594.

[11] A. Farughian, L. Kumpulainen, K. Kauhaniemi, Review of methodologies for earth fault indication and location in compensated and unearthed MV distribution networks, Electr. Power Syst. Res. 154 (2018) 373–380.

[12] P. Liu, C. Huang, Detecting single-phase-to-ground fault event and identifying faulty feeder in neutral ineffectively grounded distribution system, IEEE Trans. Power Deliv. 33 (5) (2018) 2265–2273.

[13] M. Lukowicz, W. Rebizant, M. Kereit, New approach to intermittent earth fault detection with admittance criteria, Int. J. Electr. Power Energy Syst. 123 (2020) 106271.

[14] G. Druml, New method for measuring the earthfault-distance in compensated and isolated networks, in: CIRED 2021-26th Int. Conf. Exhib. Electricity Dist, 2021, pp. 1–4.

[15] W. Zhang, X. Xiao, Y. Wang, T. Zheng, H. Zhao, H. Wang, Charging-transient based SLG fault location in neutral-unearthed distribution system, in: 2011 Asia-Pacific Power and Energy Engineering Conference, 2011, pp. 1–4.

[16] G. Druml, Results from the new method for measuring the earthfault-distance in compensated and isolated networks, in: 16th Int. Conf. Developments in Power System Protection, DPSP 2022, 2022, pp. 1–4.

[17] C. Galvez, A. Abur, Fault location in meshed and active power distribution networks, in: 2021 IEEE Madrid PowerTech, 2021, pp. 1–6.

[18] T.A. Zerihun, T. Treider, H. Taxt, L.B. Nordevall, T.S. Haugan, Two novel current-based methods for locating earth faults in unearthed ring operating MV networks, Electr. Power Syst. Res. 213 (2022) 108774.

[19] M. Biller, J. Jaeger, Protection algorithms for closed-ring grids with distributed generation, IEEE Trans. Power Deliv. 37 (5) (2022) 4042–4052.

[20] D. Wolter, M. Zdrallek, M. Stötzel, C. Schacherer, I. Mladenovic, M. Biller, Impact of meshed grid topologies on distribution grid planning and operation, in: CIRED 2017-24th Int. Conf. Exhib. Electricity Dist, 2017, pp. 2338–2341.

[21] M. Wadi, M. Baysal, A. Shobole, Comparison between open-ring and closed-ring grids reliability, in: 2017 4th Int. Conf. on Electrical and Electronic Engineering, ICEEE, Ankara, Turkey, 2017, pp. 290–294.

[22] M. Wadi, M. Baysal, A. Shobole, Reliability and sensitivity analysis for closed-ring distribution power systems, Electr. Power Compon. Syst. 49 (6–7) (2021) 696–714.

[23] R. Willheim, R. Waters, Transient phenomena associated with ground faults in three-phase systems, in: Neutral Grounding in High-Voltage Transmission, Elsevier, New York, NY, USA, 1956, pp. 198–200, ch. 3.

[24] T. Welfonder, Localisation de défauts monophasés dans les réseaux de distribution à neutre compensé (Ph.D. dissertation), Energie électrique, Institut National Polytechnique de Grenoble INPG, Grenoble, 1998.

[25] M. Lehtonen, Transient Analysis for Ground Fault Distance Estimation in Electrical Distribution Networks (Ph.D. dissertation), Technical Research Centre of Finland, Espoo, 1992.

[26] M. Loos, Single Phase to Ground Fault Detection and Location in Compensated Network (Ph.D. dissertation), Université Libre De Bruxelles, Brussels, 2014.

[27] M.F. Abdel-Fattah, M. Lehtonen, R.J. Millar, C.J. Kim, The impact of the distribution network type and configuration on the transient behavior of the fault and neutral points during earth faults, in: Int. Conf. on Power Systems Transients, Vol. 21, IPST2011, pp. 1–8.

[28] J.A. Martinez-Velasco (Ed.), Power System Transients: Parameter Determination, Taylor & Francis Group, Boca Raton, FL, USA, 2010.

[29] T. Noda, Numerical techniques for accurate evaluation of overhead line and underground cable constants, IEEJ Trans. Electr. Electron. Eng. 3 (5) (2008) 549–559.

[30] E.S. Bañuelos-Cabral, J.A. Gutiérrez-Robles, J.L. García-Sánchez, J. Sotelo-Castañón, V.A. Galván-Sánchez, Accuracy enhancement of the JMarti model by using real poles through vector fitting, Elect. Eng. 101 (2019) 635–646.

[31] B. Gustavsen, A. Semlyen, Admittance-based modeling of transmission lines by a folded line equivalent, IEEE Trans. Power Deliv. 24 (1) (2009) 231–239.

[32] J.S.L. Colqui, L.C. Timaná, P.T. Caballero, S. Kurokawa, J.P. Filho, A modified implementation of the Folded Line Equivalent transmission line model in the Alternative Transient Program, Electr. Power Syst. Res. 211 (2022) 108185.

[33] H.K. Høidalen, L. Prikler, F. Peñaloza, ATPDRAW version 7.3 for windows - users' manual, 2021.

[34] A. Nikander, E. Lakervi, J. Suontausta, Applications of transient phenomena during earth-faults in electricity distribution networks, in: Proceedings 1995 International Conference on Energy Management and Power Delivery, Vol. 1, EMPD '95, Singapore, 1995, pp. 234–239.

[35] Short-circuit currents in three-phase a.c. systems - Part 0: Calculation of currents, 2016, IEC 60909-0:2016.

[36] K. Pandakov, Improvements in Protection of Medium Voltage Resonant Grounded Networks with Distributed Sources (Ph.D. dissertation), Department of electric power engineering, Norwegian University of Science and Technology, Trondheim, Norway, 2018.